# Title: Sensitive Electromechanical Sensors Using Viscoelastic Graphene-Polymer Nanocomposites

**Authors:** Conor S Boland,[1] Umar Khan,[1] Gavin Ryan,[1] Sebastian Barwich,[1] Romina Charifou,[1] Andrew Harvey,[1] Claudia Backes,[1] Zheling Li,[2] Mauro S Ferreira,[1] Matthias E Möbius,[1] Robert J Young,[2] Jonathan N Coleman[1]*

**Affiliations:**

[1]School of Physics, CRANN and AMBER Research Centers, Trinity College Dublin, Dublin 2, Ireland

[2]National Graphene Institute and School of Materials, The University of Manchester, Manchester, M13 9PL, United Kingdom

*Correspondence to: colemaj@tcd.ie

**Abstract**: Despite its widespread use in nanocomposites, the effect of embedding graphene in highly viscoelastic polymer matrices is not well-understood. We add graphene to a lightly cross-linked polysilicone, often encountered as Silly Putty®, changing its electro-mechanical properties significantly. The resulting nanocomposites display unusual electromechanical behavior such as post-deformation temporal relaxation of electrical resistance and non-monotonic changes in resistivity with strain. These phenomena are associated with the mobility of the nanosheets in the low-viscosity polymer matrix. By considering both the connectivity and mobility of the nanosheets, we develop a quantitative model that completely describes the electromechanical properties. These nanocomposites are sensitive electromechanical sensors with gauge factors >500 which can measure pulse, blood pressure and even the impact associated with the footsteps of a small spider.

**One Sentence Summary:** Adding graphene to a viscoelastic polymer results in unexpected electromechanical properties and impressive sensing capability.

**Main Text:**

There is widespread interest in graphene because of its exceptional physical properties(*1*). An important application area involves the addition of graphene to polymers, usually to enhance electrical, mechanical or barrier properties(*2*). One important property of polymers is viscoelasticity: their mechanical properties demonstrate a combination of viscous and elastic properties, resulting in interesting time-dependent phenomena(*3*). Although the rheology of graphene-polymer nanocomposites has been investigated(*4*), the effects of viscoelastic matrices- in particular the implications of very low matrix viscosities- have not been explored.

Here we study the effect of adding graphene to a lightly cross-linked silicone polymer (commonly found as the novelty material "silly putty"), that is a highly viscoelastic material under ambient conditions(*5*). Addition of graphene to the polymer renders it conductive and increases its stiffness. However, it retains its viscoelasticity characteristics and due to the low matrix viscosity the nanosheets are mobile and respond to deformation in a time-dependent manner. In particular, they form mobile networks that break and reform during mechanical deformation. This has led to the development of a high performance sensing material, G-putty, that can monitor deformation, pressure and impact at a level of sensitivity that is so precise that it even allows even the footsteps of small spiders to be monitored.

Graphene was prepared by liquid-phase-exfoliation of graphite in *N*-methyl-pyrrolidone(*6*), giving nanosheets with lengths ~200-800 nm (Fig. 1 A-B). The nanosheets were then transferred to chloroform and mixed with home-made "silly putty": silicone oil (Fig. 1B, inset) crosslinked with

boric acid (see (*7*) including Figs. S1-S5). While the pristine putty was adhesive, malleable and somewhat liquid-like, addition of graphene gave a stiffer, more solid-like material (Figs. 1C, S6-8, S16, S25). SEM imaging showed the G-putty to contain large quantities of nanosheets arranged in a dense, uniform and isotropic network (Fig. 1D and S7). The electrical conductivity of the G-putty increased strongly with graphene content, reaching ~0.1 S/m at ~15 vol% (Fig. 1E). According to percolation theory, the nanocomposite conductivity scales with filler volume fraction, $\phi$, as(*8*):

$$\sigma_e \propto (\phi - \phi_{c,e})^{n_e} \quad (1)$$

where $\phi_{c,e}$ and $n_e$ are the percolation threshold and exponent. This equation fits the data well, giving $\phi_{c,e}$=1.75 vol% and $n_e$=11.9. While the percolation threshold is roughly as expected(*9*), the exponent is large, consistent with a broad distribution of inter-sheet junction resistances(*10*). Detailed analysis of the mechanical properties of G-putty show it to display viscoelastic behavior, consistent with the standard linear solid model (see (*7*) including Fig. S1, Figs. S9-14 and S22-24)(*5*). All mechanical properties change with graphene content: for example the stiffness increases as a power law (Figs. 1F and S11).

Most relevant are the rheological properties. Shown in Fig. 2A are typical plots of storage (*G'*) and loss (*G''*) modulus versus oscillatory strain amplitude, $\gamma_0$ (Figs. S15-21 for all rheological data). While both *G'* and *G''* increase with graphene content (Figs. 2B and S15), the *G' vs.* $\phi$ behavior can be analyzed via the cluster-cluster-aggregation model that treats the filler network as a fractal object giving(*11*, *12*)

$$G' - G'_{poly} \propto \phi^{(3+d_B)/(3-d_N)} \quad (2)$$

where $d_N$ and $d_B$ are the fractal dimensions of the network and its backbone respectively(*12*). As expected the data follows a power law with exponent of 3.1±0.5.

While both *G'* and *G''* are invariant with strain for the putty, they both tend to fall with increasing strain amplitude for all nanocomposites. For filled elastomers, this is known as the Payne effect(*13*) and has been explained by Kraus(*11, 14*) via the strain-dependent breaking/reforming of inter-particle connections in the filler network. Then, the number density of connections depends on $\gamma_0$ as

$$N = N_0\left[1+(\gamma_0/\gamma_c)^{2m}\right]^{-1} \quad (3)$$

where $N_0$ is the initial connection density, $m$ is the network structure factor and $\gamma_c$ is the yield strain. This leads to the equation(*11*):

$$G'(\gamma_0) = G'_\infty + \frac{G'_0 - G'_\infty}{1+(\gamma_0/\gamma_c)^{2m}} \quad (4)$$

where $G'_0$ and $G'_\infty$ are the storage moduli in the limit of low and high frequencies. This model fits the data extremely well (Figs. 2A and S17-18). Extracting $\gamma_c$ and plotting *vs.* $\phi$ in Fig. 2G shows a power-law with exponent -1.71±0.3. Such behavior is consistent with the prediction of Shih *et al*. for fractal particulate networks(*12*):

$$\gamma_c \propto \phi^{-(1+d_B)/(3-d_N)} \quad (5)$$

Combining the fits in Figs. 2B and C allows us to estimate $d_B$=1.4±0.2 and $d_N$=1.6±0.2, similar to carbon-black composites(*11*), but somewhat smaller than values of ~2 found for nanoclay networks(*15*). In addition, the Krauss fits give structure factors close to $m$=0.5 which is typical for

filled elastomers (Fig. 2D)(*11*). These are consistent with the value of $m$=0.46 predicted by the Huber-Vilgis model(*11*):

$$m = (2 + d_N - d_B)^{-1} \quad (6)$$

supporting the validity of this analysis.

Of particular interest is the extremely low dynamic viscosity, $\eta' = G''/\omega$, of the matrix (Fig. 2E). Although the viscosity increases with $\phi$ as a power law (Fig. S21), the zero-shear viscosity of the putty is low compared to solid polymers at ~3000 Pa.s, consistent with its highly viscoelastic liquid-like nature. Such low viscosity may allow an unusual degree of nanosheet mobility. We can test this by applying a tensile step strain (2%) to the G-putty and monitoring the graphene network relaxation via its electrical resistance (Figs. 2F and S25). The resistance increases sharply on application of the strain before decaying slowly as a power law (Fig. 2H inset). The resistance decay is very slow compared to the stress relaxation (τ~1 s, Fig. S22-24) with the power law indicating that a wide range of decay times are involved (Fig. S25-26)(*16*). We interpret this behaviour as the strain rapidly deforming the network and breaking nanosheet-nanosheet connections, thus increasing the resistance. However, due to the low matrix viscosity, the nanosheets are somewhat mobile, and may move by diffusion or in response to the applied field via induced dipoles (Fig. S27-33). This allows the network to slowly relax, re-forming connections and giving a resistance decrease. This network relaxation can be thought as a self-healing process. Such filler mobility is unprecedented in nanocomposites at room temperature (Fig. S27). However, it also represents plasticity, meaning deformations are not fully reversible (Fig. S32).

We have characterized the electrical response the G-putty to tensile and compressive deformation (Fig. 3A). In all cases (Figs. S34-43) the fractional resistance change, $\Delta R/R_0$, increased linearly at

low strain before decreasing rapidly at higher strain, always falling below its initial value. This is significantly different to the normally observed monotonic increase of $\Delta R/R_0$ with strain(*17, 18*). The initial linear increase in $\Delta R/R_0$ with $\varepsilon$ means the G-putty can be used as a strain sensor. The sensitivity, *G*, (defined at low strain by $\Delta R / R_0 = G\varepsilon$ ) is plotted versus $\phi$ in Fig. 5E. As $\phi \to \phi_{c,e}$ *G* increases significantly(*17*), reaching $\langle G \rangle$=535 at 6.8 vol% for tensile measurements. These values surpass those of most strain sensors (nanocomposite sensors usually have *G*<40, Fig. S58)(*17, 18*).

To understand this unusual behavior mechanistically, we plot resistivity (calculated assuming constant volume), $\rho$, versus strain, observing a resistivity increase at low strain followed by a large decrease (Figs. 3C and S44-48). Having considered other models, we propose that deformation of the nanosheet network, modifies its connectivity and so its resistivity (see (*7*) including Supplementary section S4 and Figs S2-S5). We write the number density of inter-nanosheet connections as the sum of a term analogous to equation 3 ( $N_1 = N_0\left[1+(\varepsilon/\varepsilon_c)^{2m}\right]^{-1}$ ) and a term representing the reformation of connections due to diffusive or field-driven mobility of the nanosheets ( $N_2 = k_2 t$ ). Combined with a modified percolation-type relation, $\rho \propto (N_1 + N_2)^{-n_\varepsilon}$ ($n_\varepsilon$ is a scaling exponent) and using $\dot{\varepsilon} = \varepsilon / t$ gives:

$$\frac{\rho}{\rho_0} = \left[\left(1+\left(\frac{\varepsilon}{\varepsilon_c}\right)^{2m}\right)^{-1} + \frac{\varepsilon}{\varepsilon_t}\right]^{-n_\varepsilon} \qquad (7)$$

where $\varepsilon_t = \dot{\varepsilon} N_0 / k_2$. We find this expression fits the low-strain data extremely well in all cases (Fig. S44-50). Importantly the fit-values of *m* cluster around 0.5 as expected (Fig. 3D).

Equation 7 leads to an expression for *G* (see (*7*) including Supplementary section S4):

$$G = 2 + \frac{n_\varepsilon}{\varepsilon_c} - \frac{n_\varepsilon}{\varepsilon_t} \tag{8}$$

that we can apply, using the fit parameters associated with equation 7. As shown in Fig. 3B, the calculated and measured values for G match very well. Interestingly, we find that both $n_\varepsilon$ and G increase as the polymer molecular weight and hence viscosity decrease (Fig. S51).

With these properties, G-putty is a high performance electromechanical sensing material that can sense joint motion, breathing and heartbeat (Fig. 4 A-C, Fig S52). Notably, when mounted on the carotid artery, the G-putty acts as a pressure sensor outputting a waveform representing the aortic pressure, allowing pulse monitoring (Fig. 4C). The unprecedented sensitivity of G-putty allows resolution of the characteristic double peak and dichrotic notch. By careful calibration (see (*7*) including supplementary section S11, Figs. S53-57)) the peak-to-peak amplitude of the waveform can be converted to pulse (blood) pressure finding the expected value of ~40 mmHg.

We also tested the G-putty as an impact sensor by dropping balls of different mass, *m*, into a thin putty sheet from different heights, *h*. The resultant resistance waveforms show a rapid jump on impact followed by a power law decay (Fig. 4D), consistent with equation 7 (see (*7*) including supplementary section S5). The peak change in $\Delta R / R_0$ scales with impact energy ($E_{mgh} = mgh$, Fig. 4E). We can understand this by considering the conversion of kinetic energy to elastic energy of the network and using equation 7 to translate the resultant strain into a resistance change (see (*7*) including Supplementary section S5), finding:

$$\frac{\Delta R}{R_0} \approx \frac{n_\varepsilon}{W}\left(\frac{2E_{mgh}}{\varepsilon_c^{\,2} E y_0}\right)^m \tag{9}$$

where $W$ and $y_0$ are the width and thickness of the putty sensor and $E$ is the putty stiffness. Fitting the data in Fig. 4E to equation 9 gives $m$=0.5 as expected and $n_\varepsilon / \varepsilon_c$ ~5 and so $G$~7, in reasonable agreement with the compression data in Fig. 3B (Fig. S49). To highlight the potential of G-putty as an impact sensor, we caught a small spider (mass~20 mg, Fig. 4F inset) and induced it to walk over a clingfilm-coated G-putty sensor. The resultant resistance plot is presented in Fig. 4F and shows individual spider footsteps, demonstrating the high sensitivity of this material.

In summary, adding graphene to a highly viscoelastic polymer gives a composite with unprecedented electromechanical properties characterized by mobile nanosheets and non-monotonic resistance changes as the material is strained. The nanocomposites are extremely sensitive electromechanical sensors that will find applications in a range of devices.

Figures:

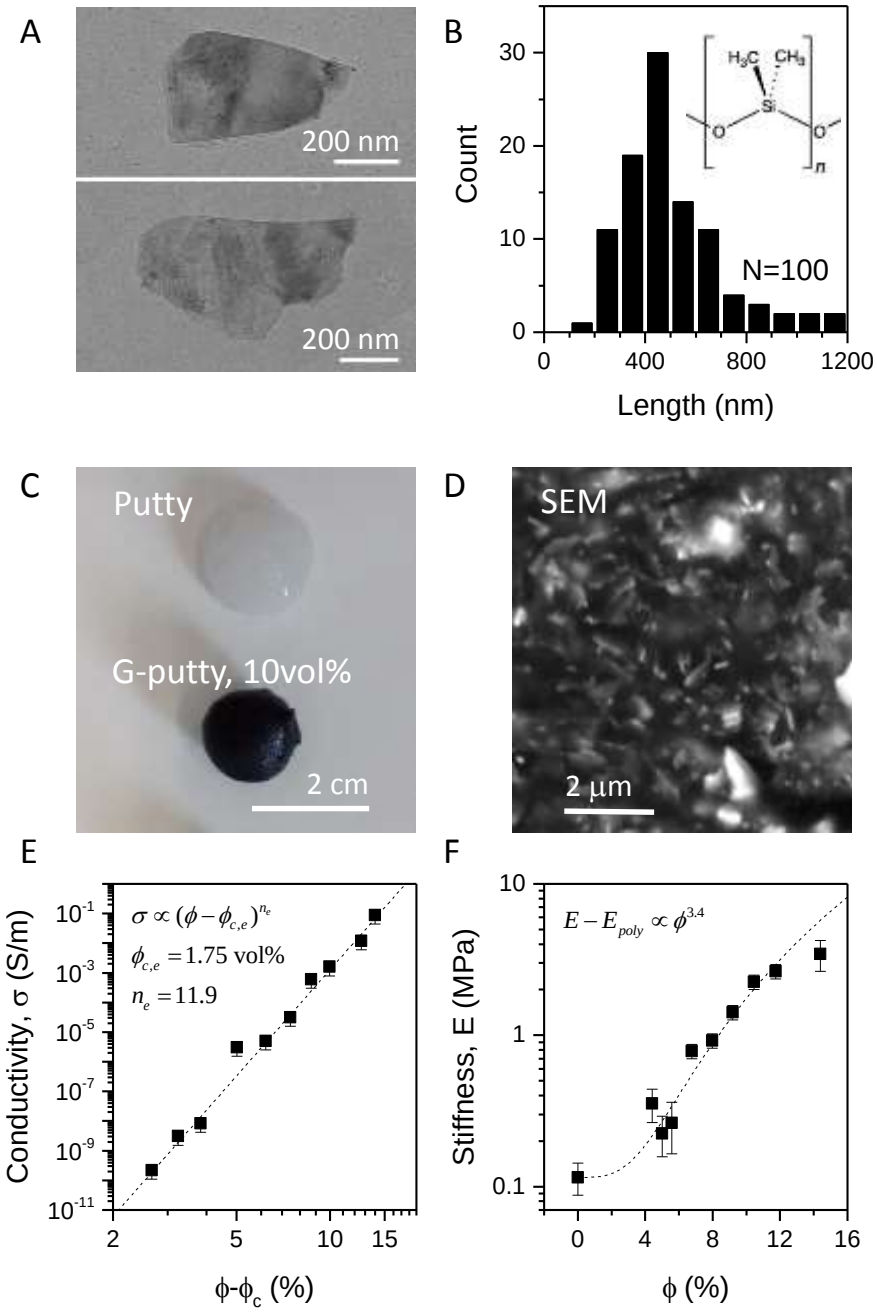


**Fig. 1**: Basic characterization of G-putty. A) TEM images and B) histogram of nanosheet length for liquid-exfoliated graphene. Inset: Structure of silicone oil. C) Photograph of hand-rolled spheres of putty and G-putty. D) SEM image of the surface of G-putty (4 vol%) showing a network

of graphene sheets. E) Electrical conductivity of G-putty as a function of reduced graphene volume fraction, $\phi$-$\phi_c$, where $\phi$ is the volume fraction and $\phi_c$ is the electrical percolation threshold. F) Mean compressive stiffness (average of 5 measurements±SD), plotted versus $\phi$.

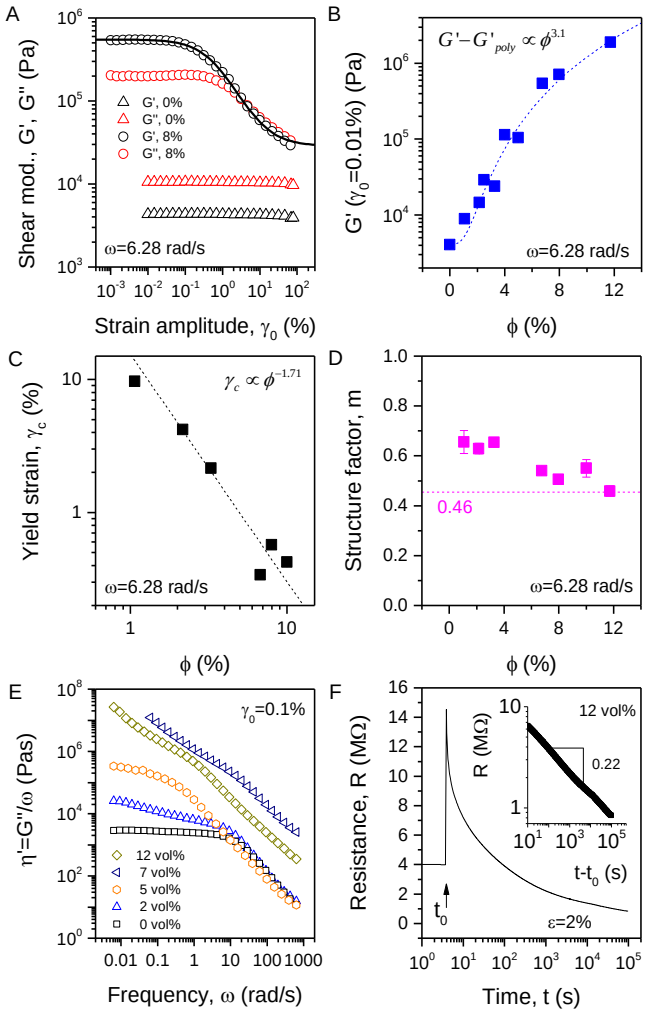


**Fig. 2**: Rheology of G-putty. A) Shear storage ($G'$) and loss ($G''$) moduli for putty and an 8 vol% composite measured as a function of shear strain amplitude, $\gamma_0$ ($\gamma = \gamma_0 e^{i\omega t}$). The composite storage modulus curve has been fit to equation 4. B) $G'$ ($\omega$=6.28 rad/s, $\gamma_0$=0.01%) plotted versus $\phi$. The dashed line is a fit to equation 2. C-D) Yield strain (C) and structure factor (D) as extracted from

the Krauss fits (equation 4), plotted versus $\phi$. The lines in C and D represent a fit to equation 5 and the value predicted by equation 6 respectively. Uncertainties in C and D are fitting errors. E) Dynamic viscosity, plotted versus $\omega$ for a range of graphene contents. F) Time evolution of electrical resistance of G-putty ($\phi$=11.7%) exposed to a 2% tensile step strain at $t=t_0$. Inset: log-log plot.

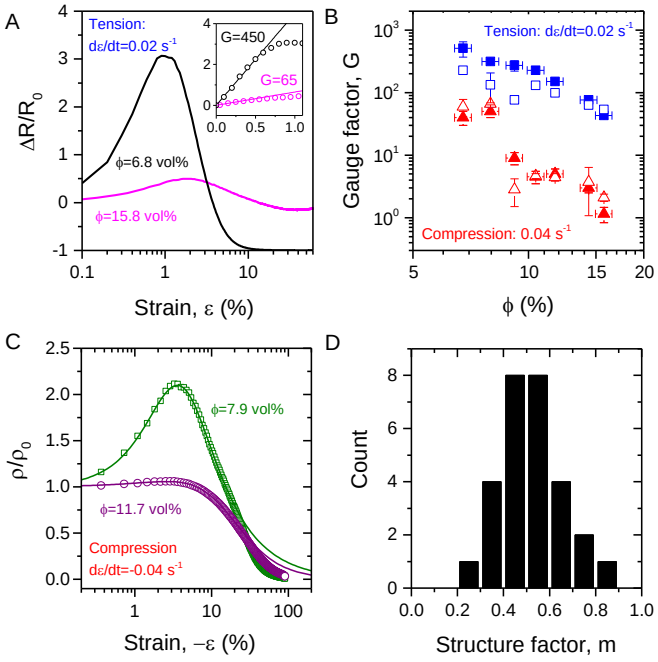


**Fig. 3**: Electromechanical properties of G-putty. A) Fractional resistance change for G-putty as a function of tensile strain. Inset: Low strain regime. B) Mean (over 5 measurements±SD) gauge factor plotted versus volume fraction for both tensile (blue) and compressive (red) measurements. The solid and open symbols represent measured and predicted (equation 8) data respectively. C) Normalized resistivity as a function of strain measured in compression for two volume fractions. The lines are fits to equation 7. D) Histogram showing all values of *m* found by fitting data using equation 7.

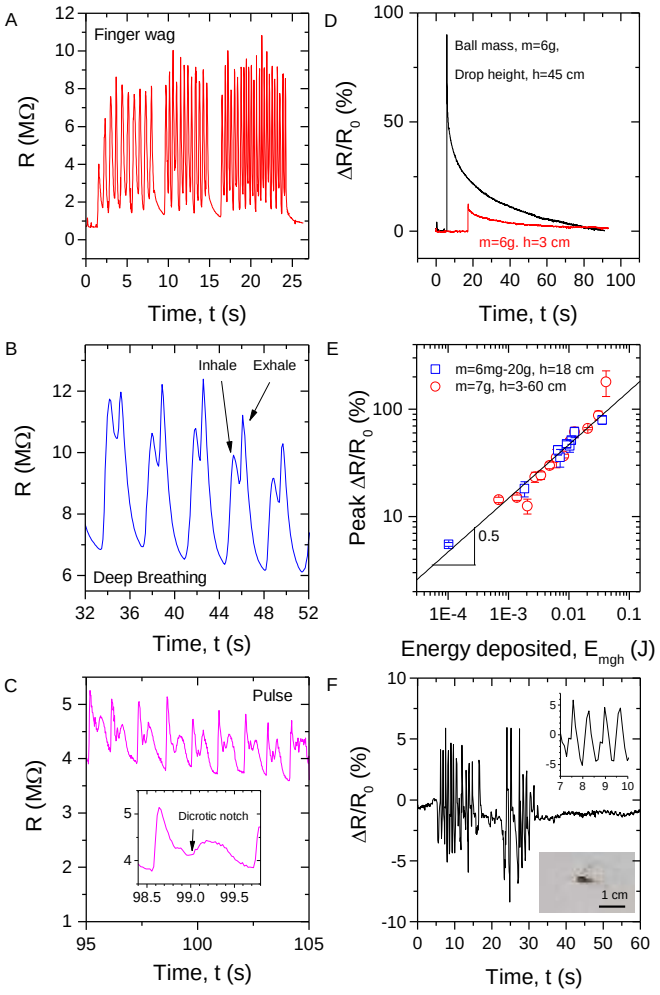


**Fig. 4**: Mechanical sensing applications of G-putty ($\phi$=6.8 vol%). A-C) Resistance waveforms measured while using G-putty to sense finger joint motion (wagging, A) breathing (B) and pulse (C). The inset in (C) shows a single period of the pulse-waveform with the characteristic dicrotic notch indicated. D) Fractional resistance change of flat G-putty strips (thickness $y_0$=2 mm) on impact from falling metal balls. E) Peak $\Delta R/R_0$ plotted versus energy deposited by the falling ball (calculated from $E_{mgh}=mgh$). The line is a fit to equation 9. H) Fractional resistance change associated with a spider (*Pholcus phalangioides* or cellar spider, see lower inset) walking across a

thin circular sheet of G-putty (thickness $y_0$= 2 mm). Upper inset: magnified response showing individual footsteps.

**Supplementary Materials:**

Materials and Methods

Standard Linear Solid Rheological model

*R*-strain model

Impact detection model

Supplementary Data

Figs. S1-S58

Table S1

## References and Notes


1. K. S. Novoselov *et al.*, A roadmap for graphene. *Nature* **490**, 192-200 (2012).
2. R. J. Young, I. A. Kinloch, L. Gong, K. S. Novoselov, The mechanics of graphene nanocomposites: A review. *Compos. Sci. Technol.* **72**, 1459-1476 (2012).
3. R. J. Young, P. A. Lovell, *Introduction to polymers*. (CRC Press, Boca Baton, 2011).
4. S. N. Tripathi, R. S. Malik, V. Choudhary, Melt rheology and thermomechanical behavior of poly(methyl methacrylate)/reduced graphene oxide nanocomposites. *Polym. Adv. Technol.* **26**, 1558-1566 (2015).
5. R. Cross, Elastic and viscous properties of silly putty. *Am. J. Phys.* **80**, 870-875 (2012).
6. Y. Hernandez *et al.*, High-yield production of graphene by liquid-phase exfoliation of graphite. *Nat. Nanotechnol.* **3**, 563-568 (2008).
7. See supplementary materials on Science Online
8. D. S. Stauffer, A. Aharony, *Introduction to percolation theory*. (Taylor and Francis, London, 1994).
9. S. Stankovich *et al.*, Graphene-based composite materials. *Nature* **442**, 282-286 (2006).
10. P. M. Kogut, J. P. Straley, Distribution-induced non-universality of the percolation conductivity exponents. *J. Phys. C* **12**, 2151-2159 (1979).
11. G. Heinrich, M. Kluppel, *Recent advances in the theory of filler networking in elastomers:. Filled elastomers drug delivery systems* (2002), vol. 160, pp. 1-44.
12. W. H. Shih, W. Y. Shih, S. I. Kim, J. Liu, I. A. Aksay, Scaling behavior of the elastic properties of colloidal gels. *Phys. Rev. A* **42**, 4772-4779 (1990).
13. A. R. Payne, The dynamic properties of carbon black-loaded natural rubber vulcanizates. *J. Appl. Polym. Sci.* **6**, 57-63 (1962).
14. G. Kraus, Mechanical losses in carbon-black-filled rubbers. *J. Appl. Polym. Sci. Symp.*, 75-92 (1984).
15. J. Vermant, S. Ceccia, M. K. Dolgovskij, P. L. Maffettone, C. W. Macosko, Quantifying dispersion of layered nanocomposites via melt rheology. *J. Rheol.* **51**, 429-450 (2007).
16. H. H. Winter, M. Mours, *Rheology of polymers near liquid-solid transitions. Neutron spin echo spectroscopy viscoelasticity rheology* (Springer-Verlag Berlin Heidelberg, 1999), pp. 165-234.
17. J. Zhao, G.-Y. Zhang, D.-X. Shi, Review of graphene-based strain sensors. *Chin. Phys. B* **22**, 057701 (2013).
18. C. S. Boland *et al.*, Sensitive, high-strain, high-rate bodily motion sensors based on graphene-rubber composites. *ACS Nano* **8**, 8819-8830 (2014).



Acknowledgements: We acknowledge the Science Foundation Ireland-funded AMBER research centre (SFI/12/RC/2278). JNC and RJY acknowledge funding from the European Union Seventh Framework Program under grant agreements n°604391 and n°696656 Graphene Flagship. 'Graphene Polymer Nanocomposites' filed at the EPO (EP16182749.8) on 4th August 2016 – Inventors Jonathan N Coleman, Umar Khan and Conor Boland – Assignee: Trinity College Dublin.